

RESEARCH ARTICLE

Improving the performance of a chaotic nonlinear system of fractional-order brushless direct current electric motor using fractional-order sliding mode control

Amin Kaveh¹, Mohammad Vahedi^{2*}, and Majid Gandomkar¹

¹Department of Electrical Engineering, College of Technical, Islamic Azad University, Saveh, Iran

²Department of Mechanical Engineering, College of Technical, Islamic Azad University, Saveh, Iran
Amin.kaveh@iau.ac.ir, Mo.Vahedi@iau.ac.ir, majid.gandomkar@iau.ac.ir

ARTICLE INFO

Article History:

Received: January 14, 2025

Revised: March 7, 2025

Accepted: March 24, 2025

Published Online: April 22, 2025

Keywords:

Brushless direct current motor

Fractional-order sliding mode control
Chaos

Lyapunov stability

Robust control

AMS Classification 2010:

34A08, 26A33, 34H10, 93C10

ABSTRACT

Brushless direct current (BLDC) motors are widely used in industrial applications due to their high efficiency and reliability. However, these motors exhibit inherent nonlinear and chaotic behavior, which can degrade performance and cause instability under certain operating conditions. This paper proposes a fractional-order sliding mode controller (FO-SMC) for robust chaos suppression and improved stability in BLDC motor systems to address this issue. The proposed controller leverages fractional-order calculus to enhance robustness, mitigate chattering, and provide better disturbance rejection than conventional control approaches. A comprehensive Lyapunov-based stability analysis is conducted to ensure finite-time convergence and system stability under parameter uncertainties and external disturbances. The effectiveness of the proposed FO-SMC is evaluated through extensive numerical simulations, comparing its performance against the integer-order sliding mode control method. The results demonstrate that FOS-MC significantly outperforms traditional controllers regarding settling time, overshoot reduction, and robustness to external perturbations. Additionally, the study explores the practical feasibility of implementing the proposed control strategy in real-time applications using Grunwald–Letnikov fractional derivatives, which enable efficient numerical approximation and digital implementation in field-programmable gate array-based and microcontroller-driven control systems. The findings confirm that FOS-MC provides a highly adaptive and resilient solution for stabilizing BLDC motors, making it a strong candidate for advanced industrial automation and high-performance motor control applications.



1. Introduction

Nowadays, vehicles are increasingly being equipped with permanent magnet synchronous motors. One of the most widely used motors in industrial applications is the brushless direct current (BLDC) motor, which is particularly favored in the automotive industry due to its sensorless operation. These motors provide maximum torque at a standstill, and their torque

decreases linearly with increasing speed. However, due to the square wave shape of the current and the commutation action between the phases, they exhibit torque ripple, which can impact their performance. Various techniques have been developed to minimize torque ripple in BLDC motors.¹⁻⁴

By examining the performance of different electric motors, it is evident that conventional DC

*Corresponding Author

motors offer high efficiency but require a commutator and brushes, which demand regular maintenance. To overcome this limitation, BLDC motors have been introduced. These motors consist of a permanent magnet rotor and a stator winding similar to traditional motors, but unlike conventional DC motors, they do not require brushes for commutation, as this is managed electronically. The inverter plays the role of the commutator, making these motors more efficient and reliable.¹⁻⁴

The BLDC motors offer several technical advantages over traditional DC and induction motors, including a simple control system, minimal need for sensors, long lifespan, low maintenance, a favorable torque-speed characteristic, fast dynamic response, high efficiency, noiseless operation, and a wide speed range. These features make BLDC motors preferred for applications requiring high efficiency, low noise, and precise control. Given these benefits, BLDC motors are widely used in high-power and high-torque applications with space limitations, where their compact size, efficiency, and torque-speed characteristics make them ideal. A novel sensorless control scheme proposes a terminal sliding mode observer to replace mechanical sensors and improve speed estimation in interior permanent magnet synchronous motors, ensuring observer stability.⁵

Fractional calculus is increasingly being applied in various fields because it can provide more accurate modeling of real systems, which often exhibit fractional-order dynamics. Chaos theory is one of the key areas where fractional calculus plays a crucial role. Chaotic systems are highly sensitive to initial conditions, and disorganized behavior emerges when phase plane trajectories are globally bounded but locally unstable. It is well established that chaos does not occur in nonlinear continuous-time systems of order less than three. Typically, chaotic systems are modeled using three coupled differential equations that include fractional-order derivatives.⁶ Recent studies have demonstrated the effectiveness of fractional-order sliding mode controllers (FO-SMCs) in suppressing chaotic oscillations while improving system stability. For instance, Li et al. proposed a circulating current controller for modular multi-level converters, integrating fractional-order calculus to enhance response speed and minimize chattering.⁷

The existence of chaos in motor systems was first reported by Kuroe in 1989.^{8,9} The first mathematical model analyzing chaos and bifurcation

in permanent magnet synchronous motors was developed by Shahzad.¹⁰ In recent years, BLDC motors have been increasingly adopted in automotive, aerospace, robotics, household appliances, medical devices, food and chemical processing, electric vehicles, and computer peripherals due to their high efficiency, long lifespan, and good speed-torque characteristics.^{11,12} The chaotic behavior of BLDC motors was initially identified by Hemati,¹³ and such behavior is undesirable in engineering applications because it can degrade system performance.⁸ Consequently, numerous studies have been conducted on chaos control in BLDC systems^{14,15} and the synchronization of chaotic BLDC motors.¹⁶ Chaos in BLDC motors leads to oscillations, acoustic noise, mechanical vibrations, and increased electrical energy consumption, ultimately reducing motor lifespan. Thus, studying and controlling chaos is critical for improving motor design and performance.¹⁴⁻¹⁹

Since the 1970s, researchers have extensively studied the dynamic characteristics of electric motors, focusing on startup issues, speed control, and oscillations. These challenges, particularly low-speed oscillations in controlled-speed motors, are closely related to chaos in nonlinear systems. The mathematical models for multi-variable BLDC motors are highly nonlinear and strongly coupled, leading to complex dynamical behaviors. Advances in permanent magnet materials have further increased the use of BLDC motors in servo systems, high-performance drives, and household appliances.⁸

Various control methodologies have been proposed for chaos mitigation in BLDC systems, including proportional-integral-derivative (PID) control, fractional-order PID (FOPID) control, and sliding mode control (SMC). While FOPID controllers enhance conventional PID strategies by incorporating fractional-order terms for improved flexibility and disturbance rejection, their computational complexity necessitates advanced optimization techniques such as particle swarm optimization or genetic algorithms for parameter tuning. SMC, particularly in its fractional-order form (FO-SMC), has emerged as a more promising alternative due to its robustness against parameter uncertainties, finite-time convergence, and reduced chattering.²⁰

To comprehensively address the reviewers' concerns, this study also evaluates the potential integration of interval type-2 (IT2) fuzzy logic control (FLC) with FO-SMC for BLDC motor

control. IT2 FLC introduces a footprint of uncertainty, enhancing adaptability to nonlinearities and external disturbances compared to type-1 FLC.²¹ This method has demonstrated superior performance in uncertain and nonlinear systems, particularly in real-world BLDC motor applications where parameter variations are inevitable.²²

Despite its adaptability, IT2 FLC exhibits significantly higher computational complexity than conventional SMC and FO-SMC strategies, making it less practical for high-speed BLDC motor control. In contrast, FO-SMC leverages fractional calculus to incorporate memory effects, enabling smoother control actions and superior robustness without additional fuzzy tuning. Although IT2 FLC provides an adaptive framework, it lacks the finite-time convergence guarantees of FO-SMC, making the latter more suitable for high-precision motor control. However, a hybrid approach combining IT2 FLC and FO-SMC may offer a promising avenue for future research, merging the strengths of both methodologies.²³

Furthermore, while widely used, traditional PID controllers struggle with parameter uncertainties and external disturbances in BLDC motors.²⁴ FOPID controllers improve upon PID by offering better tuning flexibility and disturbance rejection capabilities.²² However, they still exhibit computational complexity and may fail to suppress chaotic oscillations²³ completely. To address these challenges, SMC and FO-SMC were developed as robust control alternatives. While SMC provides strong disturbance rejection and finite-time convergence, it suffers from chattering, potentially leading to mechanical wear in BLDC motors.²⁵ FO-SMC mitigates this issue by incorporating fractional calculus, achieving smoother control actions, enhanced robustness, and minimal chattering.²⁶ Simulation results confirm that FO-SMC outperforms PID, FOPID, and conventional SMC in reducing steady-state error, improving transient response, and minimizing control effort.

Recent research has also explored the hardware implementation of advanced control techniques using field-programmable gate arrays (FPGA). Huerta-Moro et al.²⁴ demonstrated that FPGA-based SMC and PID controllers for DC-DC buck converters significantly improved response time and reduced overshoot, suggesting their potential for real-time chaos suppression in BLDC motors. These findings reinforce the importance of integrating advanced controllers with efficient hardware platforms.

This study aims to design a FO-SMC to suppress chaotic behavior in a BLDC motor system.

A suitable sliding surface is designed to stabilize the system, minimize oscillations, and improve adaptability under external disturbances and parameter uncertainties. The results demonstrate the superior performance of FO-SMC in mitigating chaos while ensuring system stability and efficiency.

2. Mathematical modeling and chaos analysis

2.1. Brushless direct current electric motor system and assumptions

In this study, the dynamic characteristics of a BLDC motor were analyzed to establish a robust control strategy (Figure 1). First, the mathematical model of the system is formulated, which is essential for investigating the bifurcation and chaos analysis. The system's equilibrium points and stability properties are subsequently determined to provide insights into its nonlinear dynamics.



Figure 1. Schematic of a brushless direct current motor²⁵

A BLDC motor is powered by a DC electric source and differs from traditional DC motors by employing a closed-loop electronic controller instead of mechanical brushes. This controller converts the incoming DC current into motor coils that generate magnetic fields, enabling smooth and precise rotation. Unlike conventional

DC motors that rely on mechanical commutators, BLDC motors offer several advantages, including a higher torque-to-weight ratio, improved efficiency, greater torque output per watt, increased reliability, reduced noise, and extended lifespan due to the elimination of brush and commutator wear. Additionally, removing ionizing sparks reduces electromagnetic interference, making BLDC motors ideal for precision applications. Their efficiency is notably superior in no-load and low-load regions, primarily due to the absence of friction losses associated with brushes.^{26,27}

This study makes the following key assumptions to ensure a realistic and practical evaluation of the FO-SMC for BLDC motors:

- Bounded motor parameter uncertainty: The motor parameters (resistance, inductance, and back electromotive force coefficients) are assumed to be within a reasonable uncertainty range, aligning with manufacturer-provided tolerances. This ensures feasibility without assuming unrealistic, completely unknown parameters.
- Fractional-order dynamics for accuracy: Since BLDC motors exhibit memory-dependent behaviors, fractional-order modeling provides a more precise representation than integer-order models, ensuring better energy dissipation and hereditary effects.
- Bounded external disturbances and load variations: Practical disturbances like friction and load torque changes are naturally bounded. Assuming finite limits ensures the stability of the FO-SMC, as real-world controllers cannot compensate for unbounded disturbances.
- Grunwald–Letnikov (GL) definition for fractional derivatives: The GL method is chosen for fractional derivative computations due to its computational efficiency, direct discrete approximation, and real-time feasibility, making it widely used in electromechanical systems.
- Negligible sensor noise and quantization effects: High-precision sensors and the inherent robustness of FO-SMC minimize the impact of sensor noise, making detailed noise modeling unnecessary for this study.

The dynamic equations of a BLDC electric motor are given in the following Equation (1)^{26,27}:

$$\begin{cases} \frac{di_d}{dt} = \frac{1}{L_d} [v_d - Ri_d + \omega L_q i_q] \\ \frac{di_q}{dt} = \frac{1}{L_d} [v_q - Ri_q - \omega L_d i_d - \omega \psi_r] \\ \frac{d\omega}{dt} = \frac{1}{J} [n_p \psi_r i_q + n_p (L_d - L_q) i_d i_q - T_L - \beta \omega] \end{cases} \quad (1)$$

where (v_d, i_d) and (v_q, i_q) are the d-q voltage and current of the electric motor, L_q and L_d are the stator inductances, and R is the stator resistance. $\psi_r, \beta,$ and J are the fixed magnetic flux, friction coefficient, and polar moment of inertia. The number of pairs of poles is represented by n_p . T_L is the external load torque, and ω is the rotor angular velocity. Based on an agreement, Equation (1) is simplified using the following transformations.²⁶

Assuming $T = \begin{bmatrix} bk & 0 & 0 \\ 0 & k & 0 \\ 0 & 0 & R/L_q \end{bmatrix}$, where $b = L_q/L_d$, $k = \frac{\beta R}{L_q n_p \psi_r}$, a $\gamma = \frac{\psi_r}{k L_q}$, $\sigma = \frac{\beta L_q}{R J}$, $u_d = \frac{v_d}{R k}$, $u_q = \frac{v_q}{R k}$, $v = \frac{n_p b L_q^2 k^2 ((L_d - L_q))}{J R^2}$, $\widetilde{T}_L = \frac{L_q^2 T_L}{J R^2}$, and $t' = (R t)/L_q$. State variables are obtained as $(\widetilde{\cdot}) = T^{-1}(\cdot)$. Using these transformations, Equation (1) is obtained as the following set of dimensionless equations²⁶:

$$\begin{cases} \frac{d\widetilde{i}_d}{dt'} = u_d - \mu \widetilde{i}_d + \widetilde{\omega} \widetilde{i}_q \\ \frac{d\widetilde{i}_q}{dt'} = u_q - \widetilde{i}_q - \widetilde{\omega} \widetilde{i}_d + \gamma \widetilde{\omega} \\ \frac{d\widetilde{\omega}}{dt'} = \sigma [\widetilde{i}_q (\widetilde{i}_q - \widetilde{\omega}) + \widetilde{i}_d + v \widetilde{i}_d \widetilde{i}_q - \widetilde{T}_L] \end{cases} \quad (2)$$

such that $\sigma, \gamma, \mu,$ and v are the structural parameters of the dynamic system of the motor after transformations and are the d-q reference voltage and current of the electric motor. \widetilde{T}_L is the load torque after transformation and $\widetilde{\omega}$ is the rotor angular velocity after transformation. Assuming $\widetilde{i}_q = x_1, \widetilde{i}_d = x_2,$ and $\widetilde{\omega} = x_3$ are similar to the Lorentz system, the dynamic equations of the BLDC system are converted to the state space form:

$$\begin{cases} \dot{x}_1 = -\mu x_1 + x_2 x_3 + u_d \\ \dot{x}_2 = -x_2 - x_1 x_3 + \gamma x_3 + u_q \\ \dot{x}_3 = -\sigma (x_3 - x_2) - \widetilde{T}_L + v x_1 x_2 \end{cases} \quad (3)$$

The fractional order form of such a system is as follows^{16,28}:

$$\begin{cases} {}_0 D_t^{q_1} x_1 = -\mu x_1 + x_2 x_3 + u_d \\ {}_0 D_t^{q_2} x_2 = -x_2 - x_1 x_3 + \mu x_3 + u_q \\ {}_0 D_t^{q_3} x_3 = -\sigma (x_3 - x_2) - \widetilde{T}_L + v x_1 x_2 \end{cases} \quad (4)$$

It should be noted that considering fractional-order dynamics in many systems can significantly improve stability and increase accuracy in system behavior. The numerical solution of the fractional-order BLDC system is formulated using the GL fractional derivative, ensuring a more precise representation of the system's nonlinear dynamics. The governing fractional-order equations are expressed as follows:^{5,6}

$$\begin{cases} x_1(t_k) = -\mu x_1(t_{k-1}) + x_2(t_{k-1})x_3(t_{k-1}) \\ \quad + u_d(t_{k-1})h^{q_1} - \sum_{j=v}^k c_j^{(q_1)}x_1(t_{k-j}) \\ x_2(t_k) = -x_2(t_{k-1}) - x_1(t_k)x_3(t_{k-1}) \\ \quad + \gamma x_3(t_{k-1}) + u_q(t_{k-1})h^{q_2} \\ \quad - \sum_{j=v}^k c_j^{(q_2)}x_2(t_{k-j}) \\ x_3(t_k) = \sigma x_2(t_k) - x_3(t_{k-1}) - \widetilde{T}_L(t_{k-1}) \\ \quad + v x_1(t_k)x_2(t_k)h^{q_3} - \sum_{j=v}^k c_j^{(q_3)}x_3(t_{k-j}) \end{cases} \quad (5)$$

where T_{sim} is the simulation time, $N = [T_{sim}/h]$, and $(x_1(0), x_2(0), x_3(0), \dots)$ are the initial conditions. The numerical solution of the fractional-order BLDC system follows the GL definition, where the system's discrete representation depends on the total number of computational steps, denoted as N . This parameter is essential for ensuring numerical accuracy and stability. The estimation of N is based on the total simulation time T_{sim} and the chosen time step, defined as $N = T_{sim}/h$. The selection of h plays a crucial role in balancing accuracy and computational efficiency as a smaller h improves precision but increases the computational load, whereas a larger h reduces complexity but may lead to numerical errors or instability in chaotic systems.

The time step should be chosen carefully to maintain stability in fractional-order systems. A smaller step size ensures better differentiation accuracy but can significantly slow down computations, while a larger step size may result in approximation errors. Moreover, the memory effect in fractional calculus requires a sufficient number of computational steps to capture the long-term system behavior properly. To avoid numerical divergence, the stability constraints and eigenvalues of the system must be analyzed, ensuring that the selected h allows proper system convergence.

The binomial coefficients $c_j^{(q)}$ are computed using the GL definition⁶:

$$(c_j^{(q)} = (-1)^j \binom{q}{j} = (-1)^j \frac{\Gamma(q+1)}{\Gamma(j+1)\Gamma(q-j+1)}) \quad (6)$$

where $\Gamma(n) = \int_0^\infty t^{n-1}e^{-t}dt$, is the Gamma function. The GL definition is a fundamental approach for defining fractional derivatives and integrals. The fractional derivative of order n for a function $f(t)$ using this method is expressed as⁶:

$$\left(\frac{d^n}{dt^n}f(t) = \lim_{h \rightarrow 0} h^{-j} \sum_{j=0}^n (-1)^j \binom{n}{j} f(t-jh)\right) \quad (7)$$

This approach provides a discretized representation of fractional derivatives, making it computationally efficient for numerical simulations. It is particularly suitable for systems with memory effects and is widely used in electrical and mechanical applications, including BLDC motors. The GL approach provides a powerful framework for modeling fractional-order systems, particularly those with memory effects and long-range dependencies. Utilizing direct discretization eliminates the need for complex transformations, making it an efficient and straightforward method for numerical implementation. Moreover, its ability to capture hereditary system properties ensures accurate dynamic modeling, particularly in applications such as BLDC motors, where precise control over chaotic behavior is essential. Additionally, its computational stability makes it ideal for real-time control applications, reinforcing its superiority over other fractional-order numerical techniques. These advantages make the GL method preferred for solving fractional-order differential equations, ensuring theoretical rigor and practical feasibility in control design.

Since we are interested in the chaotic dynamics of the system, we need to focus on the equilibrium points and parameter ranges where we observe chaos. To obtain the fixed points of the system (3), we examine it for $\mu = 1$ and $v = 0$ under no-load conditions ($u_d = u_q = \widetilde{T}_L = 0$)^{3,8}

$$\begin{cases} \dot{x}_1 = -x_1 + x_2x_3 \\ \dot{x}_2 = -x_2 - x_1x_3 + \gamma x_3 \\ \dot{x}_3 = -\sigma(x_3 - x_2) \end{cases} \quad (8)$$

Therefore, we have the following in equation :

$$\dot{x}_1 = 0, \begin{cases} x_1 = 0 \\ x_1 = x_2x_3 \end{cases} \quad (9)$$

$$\dot{x}_2 = 0, \begin{cases} x_2 = 0 \\ x_2 = x_3(\gamma - x_1) \end{cases} \quad (10)$$

$$\dot{x}_3 = 0, \begin{cases} x_3 = 0 \\ x_2 = x_3 \end{cases} \quad (11)$$

By solving Equations (2.1)–(11), three fixed points are obtained. We derive these equilibrium points and discuss their local behavior.

2.2. Bifurcation and chaos in the brushless direct current system

Hopf bifurcation occurs when the corresponding Jacobian matrix has a pair of pure imaginary poles and other eigenvalues of the real part are non-zero. Here, for the BLDC system, the Hopf bifurcation and its chaotic behavior under no-load condition ($\mathbf{u}_d = \mathbf{u}_q = \widetilde{\mathbf{T}}_{\mathbf{L}} = \mathbf{0}$) are investigated. By examining Equations (2.1)–Equation (11), it is clear that $\mathbf{E}_1 = (\mathbf{0}, \mathbf{0}, \mathbf{0})$ is the first equilibrium point. And with $\gamma > 1$, two other nontrivial equilibria are $\mathbf{E}_2 = (\gamma - 1, \sqrt{\gamma - 1}, \sqrt{\gamma - 1})$ and $\mathbf{E}_3 = (\gamma - 1, -\sqrt{\gamma - 1}, -\sqrt{\gamma - 1})$. A simple analysis shows that if $0 < \gamma < 1$, the original equilibrium point is stable, and it loses its stability for $\gamma = 1$ and creates two unreal equilibrium points that are initially stable. By linearizing the system, we obtain the Jacobian matrix to discuss the local behavior of its equilibrium points. The Jacobian matrix of the system is as follows ²⁶:

$$J = \begin{bmatrix} -1 & x_3 & x_2 \\ -x_3 & -1 & -x_1 + \gamma \\ 0 & \sigma & -\sigma \end{bmatrix} \quad (12)$$

which has eigenvalues obtained by the roots of the following equation:

$$D(\lambda) = \lambda^3 + (2 + \sigma)\lambda^2 + (\sigma + \gamma)\lambda + 2\sigma(\gamma - 1) = 0 \quad (13)$$

When checked at non-origin equilibrium points (nontrivial equilibria), Since the two nontrivial equilibria are symmetric, their stability must be the same. For the bifurcation of two nontrivial equilibria, that is, the parameter values for which $\lambda = 0$ or $\lambda = j\omega$, is the solution of Equation (13). With $\lambda = 0$, we have $\gamma = 1$, which results in the bifurcation that was discussed. With $\lambda = j\omega$ and setting the real and imaginary parts equal to each other, we have the following:

$$\begin{cases} -\omega^3 + (\sigma + \gamma)\omega = 0 \\ -(2 + \sigma)\omega^2 + 2\sigma(\gamma - 1) = 0 \end{cases} \quad (14)$$

where $\omega^2 = \frac{2\sigma(\gamma - 1)}{2 + \sigma} = \sigma + \gamma$. By sorting the value of γ at which Hopf bifurcation occurs is obtained. For $\omega^2 > 0$, at this value of γ , that is:

$$\gamma_h = \frac{\sigma(\sigma + 4)}{\sigma - 2} \quad (15)$$

Which always holds for $\sigma > 2$. Therefore, the eigenvalues would be:

$$\omega^2 = \frac{2\sigma(\sigma + 1)}{\sigma - 2} > 0 \quad (16)$$

Therefore, the eigenvalues will be as follows:

$$\lambda_1 = -(\sigma + 2), \quad \lambda_{2,3} = \pm j\sqrt{\frac{2\sigma(\sigma + 1)}{\sigma - 2}} \quad (17)$$

Therefore, $\gamma = \gamma_h$ corresponds to a Hopf bifurcation point of the system and for values close to $\gamma \neq \gamma_h$, the equilibria are surrounded by the limit cycle, and for $\gamma > \gamma_h$, all three equilibria would be unstable. System (8) does not change under $(x, y, z) \Leftrightarrow (x, -y, -z)$; thus, it can be said that it is symmetric regarding the y and z axes, and if $\nabla V = \frac{\partial}{\partial x} \left(\frac{dx}{dt}\right) + \frac{\partial}{\partial y} \left(\frac{dy}{dt}\right) + \frac{\partial}{\partial z} \left(\frac{dz}{dt}\right) = -(\sigma + 2) < 0$, this system is convergent.

As mentioned before, if $\gamma \leq 1$, $E_1 = (0, 0, 0)$ is the only equilibrium point. When the system parameters change, we might expect BLDC to demonstrate stable, limited cycle, and chaotic behaviors.

As can be seen in Figure 2, $\widetilde{i}_d = x_2$ is stable for γ with initial values, but as γ increases, it tends toward chaos and instability. Because it varies a little around the original equilibrium point, but with increasing γ it goes toward chaos (irregular oscillations) and then instability. The same thing applies to the variables $\widetilde{i}_q = x_1$ and $\widetilde{\omega} = x_3$. In other words, it can be said that the parameter γ has a completely influential parameter in the system’s stability, instability, and chaos.

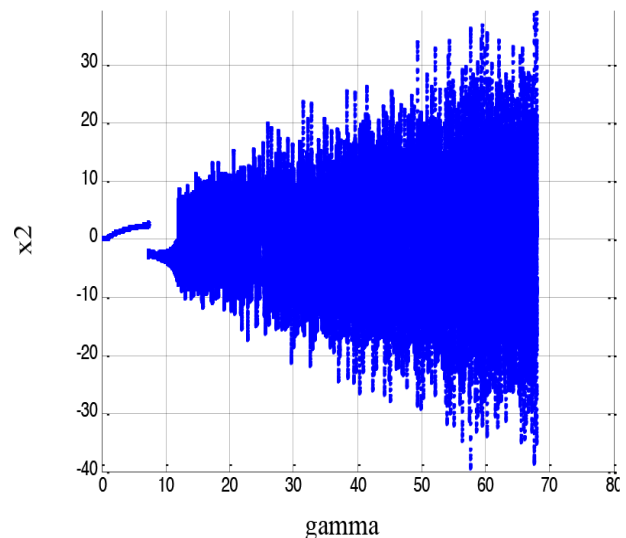


Figure 2. Bifurcation by changing γ and $\sigma = 5.4$

3. Control strategy for chaos suppression

This study considers the following assumptions to ensure the accurate modeling and practical feasibility of the proposed FO-SMC for the BLDC system.

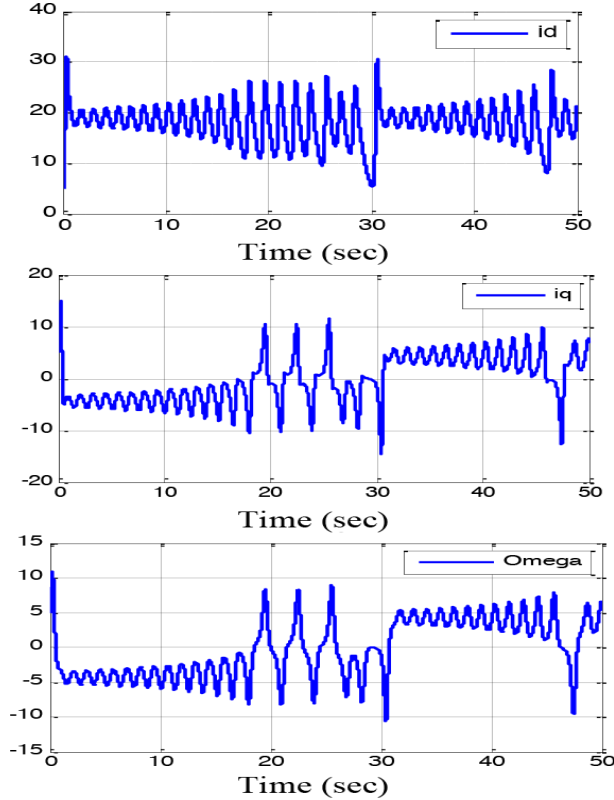


Figure 3. State variables $x_1(t)$, $x_2(t)$ and $x_3(t)$ of the fractional-order brushless direct current system without a control signal

Firstly, we analyze the FO-BLDC system under the no-load condition ($u_d = u_q = \widetilde{T}_L = 0$) and $v = 0$ in the form of Equation (4). We represent the parameter vector as $(\mu, \gamma, \text{and } \sigma) = (1, 20, \text{and } 5.46)$ and consider the system in homogeneous orders as $q_1 = q_2 = q_3 = 0.995$. To perform differentiation at the fractional order of 0.995, we can either first take the integral of the desired variable to the order of 0.005 and then take the first derivative of the result (Riemann–Liouville definition) or first take the first derivative of the function and then perform fractional-order integration of 0.005 (Caputo definition). If we do not apply any control input to the system $u(t) = 0$, it will exhibit chaotic behavior. For $T_{sim} = 50$ sec, a constant time step of $h = 0.005$, and initial conditions $(x_1(0), x_2(0), x_3(0)) = (0, 0, 0)$, the system will behave chaotically. With the above conditions, the state variables of the fractional-order BLDC system without a control signal are shown in Figure 3.

Furthermore, Figures 4 and 5 present the chaotic state trajectories of the FO-BLDC system without a control signal.

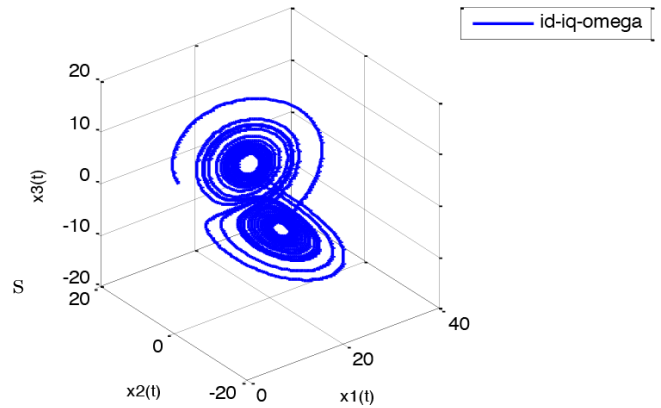


Figure 4. The chaotic state trajectories of the fractional-order brushless direct current system without control signals are represented by i_d , i_q , and ω

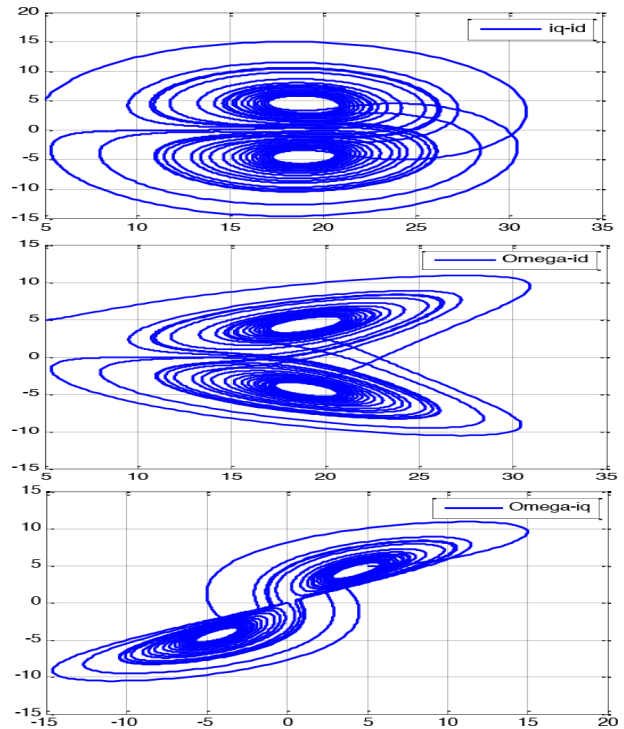


Figure 5. The chaotic state trajectories of the fractional-order brushless direct current system without a control signal are represented by $i_q - i_d$, $\Omega - i_d$ and $\Omega - i_q$

Based on this analysis, the points E_2 and E_3 represent unstable equilibrium points that satisfy the stability condition for chaotic behavior, while the point E_1 is a stable equilibrium point associated with two limit cycles.

Furthermore, when comparing the chaotic attractors of the fractional-order and conventional BLDC systems, we observe a larger stability region (attraction region) for the fractional-order system compared to the conventional one. For

instance, at a sampling time of $h = 0.005$, the fractional-order system reaches a stable equilibrium point. On the other hand, for a sampling time of $h = 0.05$, the conventional system becomes unstable from the sampling time, as illustrated in Figure 6.

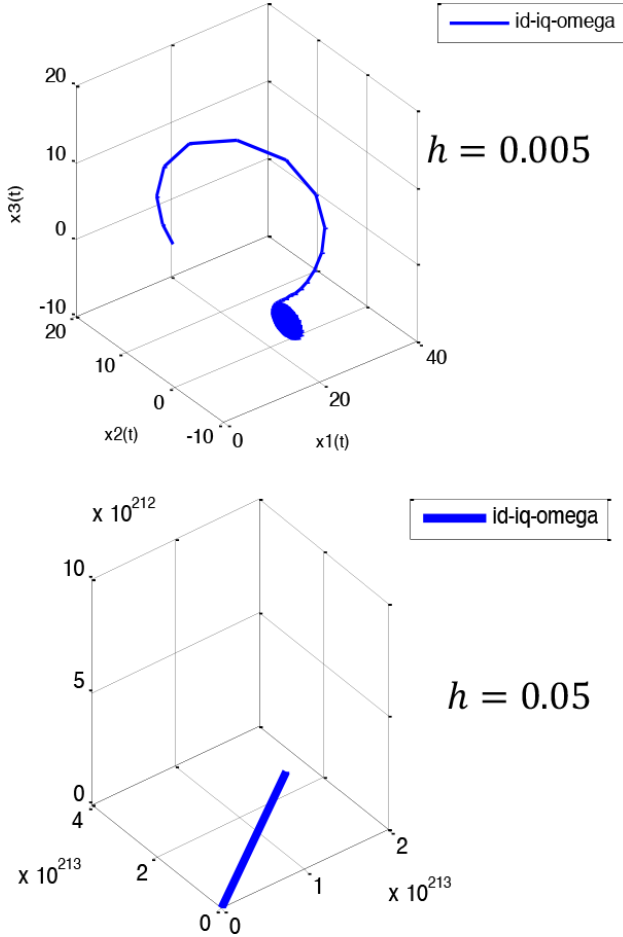


Figure 6. The chaotic state trajectories of the fractional order brushless direct current system without a control signal with $h = 0.005$ and $h = 0.05$

3.1. The fractional-order brushless direct current system with control input

We know that the fractional-order equation is represented by the following relationship:

$$\begin{cases} {}_0D_t^{q_1} x_1 = -x_1 + x_2x_3 \\ {}_0D_t^{q_2} x_2 = -x_2 - x_1x_3 + \mu x_3 \\ {}_0D_t^{q_3} x_3 = -\sigma(x_3 - x_2) \end{cases} \quad (18)$$

According to the no-load conditions and the characteristics of this section, using the trial and error method or drawing the bifurcation diagram, it can be seen that the system is unstable for $0 < q_1 = q_2 = q_3 = q < 0.6$ and $\forall q > 1.1$ conditions and when $0.6 < q < 0.98$ converges to one of the two equilibrium points of $E_2 \vee E_3$, and for $0.99 < q < 1.1$, chaotic behavior is

generated. Therefore, to stabilize this section, we consider the variable $q = 0.995$.

Considering that the controlled system is an order-fractional system, the desired sliding surface must also have an order-fractional form. We define the sliding surface such that $S \rightarrow 0$ corresponds to $x_2 \rightarrow 0$; therefore, according to the fractional-order system in Equation (18), we define the slip surface in the form of Equation (19) 29.

$$S = D_t^{q_2-1} x_2(t) \quad (19)$$

According to Equation (18), if $x_2 \rightarrow 0$, then $x_1 \rightarrow 0$ and $x_3 \rightarrow 0$, which transforms the problem into a regulation problem.

3.2. Control input design

Next, the control input u is defined as follows:⁴⁻⁶

$$u = u_{eq} + u_N \quad (20)$$

as u_{eq} is the equivalent control component, which keeps the states on the sliding surface. u_N is the switching component that directs the states to the sliding surface. u_N is primarily responsible for stabilizing the system and is designed using the Lyapunov stability criterion.

$$\begin{aligned} \dot{S}(x) &= \frac{\partial S}{\partial X} \cdot \dot{X}(t) \\ &= \frac{\partial S}{\partial X} [f(t, x) + B(t, x)(u_{eq} + u_N)] \\ &= \frac{\partial S}{\partial X} [f(t, x) + B(t, x)(u_{eq} + u_N)] \\ &= \frac{\partial S}{\partial X} [f(t, x) + B(t, x)u_{eq}] + \frac{\partial S}{\partial X} B(t, x)u_N \\ &= \frac{\partial S}{\partial X} B(t, x)u_N \end{aligned} \quad (21)$$

if we assume that $\frac{\partial S}{\partial X} B(t, x) = I$, where I is the identity matrix, then we have $\dot{S}(x) = u_N$, which satisfies this condition sufficiently.

The condition for the existence of sliding mode (condition $S_i \dot{S}_i < 0$) is given by $S \neq 0$. In the following, we will describe two important and commonly used cases in this article for the discontinuous control section:

(a) Relay with constant gain:

$$u_{iN} = \begin{cases} -\alpha_i \text{Sign}(S_i(x)), & S_i(x) \neq 0, \alpha_i > 0 \\ 0, & S_i(x) = 0 \end{cases} \quad (22)$$

where the *sign* function is meant. It is observed that choosing this option for the discontinuous

part of the control system satisfies the sliding mode condition because:

$$S_i \dot{S}_i = -\alpha_i S_i(x) \text{Sign}(S_i(x)) < 0, \quad S_i(x) \neq 0 \quad (23)$$

(b) Linear continuous feedback:

By choosing $u_{i_N}(x) = -\beta_i S_i(x)$ where ($\beta_i > 0$) as the discontinuous function, the sufficient condition for sliding mode according to the following equation is satisfied. In more general cases, the discontinuous part of the control system can be considered as a combination of the first and second cases.

$$S_i \dot{S}_i = -\beta_i S_i^2(x) < 0 \quad (24)$$

(c) Combination of the relay with a constant gain and linear continuous feedback

In general, the discontinuous control component can be considered as a combination of the first and second modes:

$$u_{i_N} = \begin{cases} -\alpha_i \text{Sign}(S_i(x)) - \beta_i S_i(x), & S_i(x) \neq 0, \alpha_i > 0, \beta_i > 0 \\ 0, & S_i(x) = 0 \end{cases} \quad (25)$$

With this choice, the sufficient condition for the discontinuous part of the control is satisfied because

$$S_i \dot{S}_i = -\alpha_i S_i(x) \text{Sign}(S_i(x)) - \beta_i S_i^2(x) < 0, \quad S_i(x) \neq 0 \quad (26)$$

Now, we denote the location of the control input in the fractional-order chaotic system:

$$\begin{cases} {}_0D_t^{q_1} x_1 = -x_1 + x_2 x_3 \\ {}_0D_t^{q_2} x_2 = -x_2 - x_1 x_3 + \gamma x_3 + u(t) \\ {}_0D_t^{q_3} x_3 = -\sigma(x_3 - x_2) \end{cases} \quad (27)$$

which $u(t)$ is the same as the combined control input. Since the sliding surface equation is defined based on the state variables according to Equation (19), the system converges to the desired state on the sliding surface.

The following equations hold on the sliding surface:

$$\begin{cases} S = 0 \\ \dot{S} = 0 \end{cases} \quad (28)$$

To obtain the equivalent control law, it suffices to substitute $\dot{S} = 0$:

$$\dot{S} = {}_0D_t^{q_2} x_2 = -x_2 - x_1 x_3 + \gamma x_3 + u_{eq}(t) = 0 \quad (29)$$

The equivalent control law $u_{eq}(t)$ is obtained as follows:

$$u_{eq}(t) = -(-x_2 - x_1 x_3 + \gamma x_3) \quad (30)$$

Now, considering the Lyapunov candidate function as a positive definite function, we have the following:

$$V = \frac{1}{2} S^2 > 0 \quad (31)$$

For asymptotic stability, the derivative of this function must be negative definite:

$$\dot{V} = S \dot{S} < 0 \quad (32)$$

This is a proposed candidate for the switching control law to satisfy Equation (32), and based on Equation (23), it is given by:

$$u_N = -\beta \text{Sign}(S(x)) - \alpha S(x) \quad (33)$$

where α and β are positive real values. By combining Equations (30) and (33) and substituting into Equation (20), the general sliding mode control law for regulating the state variables of a typical BLDC system is obtained:

$$u(t) = x_2 + x_1 x_3 - \gamma x_3 - \beta \text{Sign}(S(x)) - \alpha S(x) \quad (34)$$

4. Simulation and comparative analysis

4.1. Numerical implementation of the proposed controller

Considering the parameter vector in the form of homogeneous orders $(\mu, \gamma, \sigma) = (1, 20, 5.46)$, we model the system as $q_1 = q_2 = q_3 = 0.995$ and $T_{sim} = 50$ sec. We set the time constant $h = 0.005$ and initial conditions as $(x_1(0), x_2(0), x_3(0)) = (5, 5, 5)$. With the switching gain $k = 5$ and based on the sliding mode control input, we design a relation (32) and implement it in MATLAB software. By plotting the phase trajectories $(\dot{x} - x)$ for the reference currents $(d - q)$ of the electric motor and the rotor angular speed (ω) in both uncontrolled and controlled states, we illustrate the system behavior in a single diagram. Similarly, we plot the previously separately drawn parametric diagrams for uncontrolled and controlled states.²⁸

Figure 7 shows that the state variables and their rates of change have converged well to the zero set point. This indicates that the FO-SMC has effectively regulated the state variables of the BLDC system to the desired zero set point.

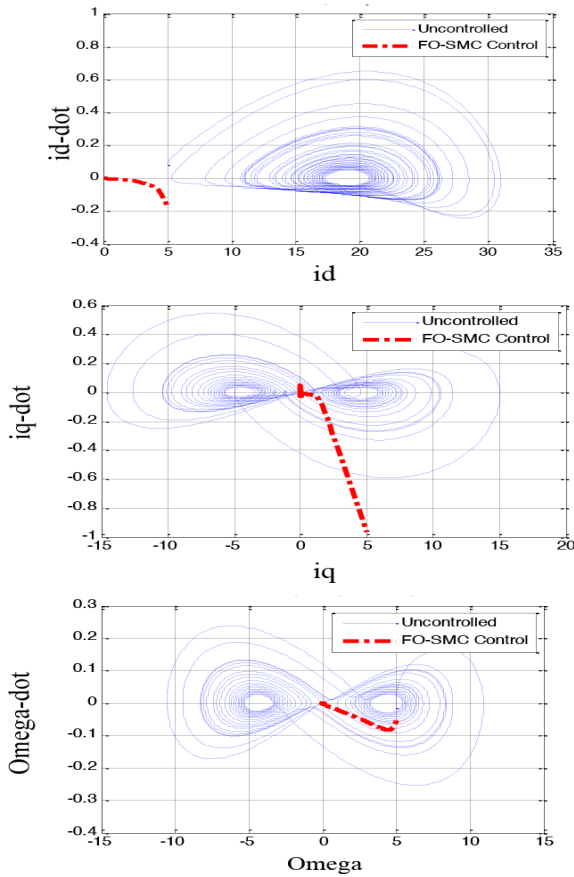


Figure 7. Phase plane diagram of state x_1 , x_2 , and x_3
 Abbreviation: FO-SMC, fractional-order sliding mode controllers

Similar to before, we consider the system in the form of homogeneous orders with respect to the parameter vector $(\mu, \gamma, \sigma) = (1, 20, 5.46)$, we model the system as $q_1 = q_2 = q_3 = 0.995$ and $T_{sim} = 6 \text{ sec}$. The time constant is $h = 0.005$, and the initial conditions are defined as $(x_1(0), x_2(0), x_3(0)) = (5, 5, 5)$. With the switching gain $k = 5$, we design relation (34) based on the sliding mode control input using the signum function and implement it in MATLAB software to plot the state trajectories, rates of change of the states, control input, and the sliding surface of the proposed method. We then compare the proposed method with conventional sliding mode control, which is applied to the system with the standard derivative, to determine the advantages of the proposed method.

Based on Figure 8, it can be observed that in the conventional sliding mode control strategy, the current i_d experiences a large overshoot at the beginning of the time, which may lead the system to saturation. On the other hand, based on this figure, it can be seen that the current i_q exhibits frequency oscillations over time in the conventional SMC strategy, which lowers the system

performance, while the proposed method is completely smooth.

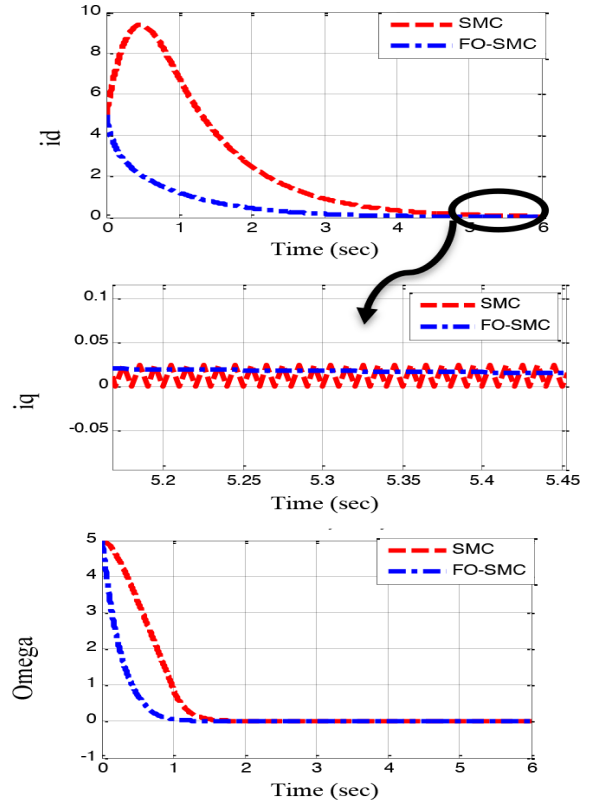


Figure 8. State trajectories regulation of i_d , i_q and Omega variables in the fractional-order brushless direct current system using the FO-SMC signal
 Abbreviations: FO-SMC, fractional-order sliding mode controllers; SMC, sliding mode controller

As shown in Figure 9, the superiority of the proposed method is somewhat evident. Based on this figure, it is apparent that the proposed FO-SMC strategy for the FO-BLDC system requires much higher initial energy control, but this range limitation can be addressed by implementing a limiter if necessary.

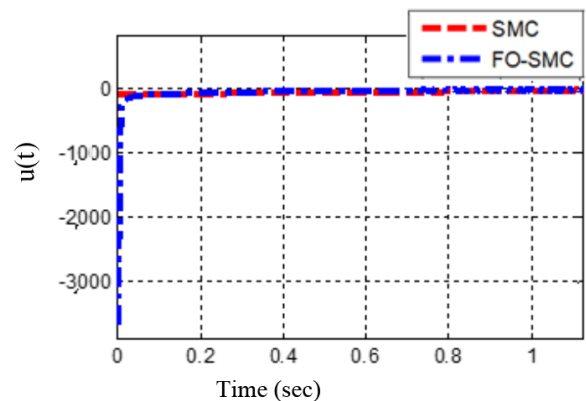


Figure 9. Control effort for state regulation of chaotic fractional-order BLDC system
 Abbreviations: BLDC, brushless direct control; FO-SMC, fractional-order sliding mode controllers; SMC, sliding mode controller

Figure 10 illustrates the sliding surface used for state regulation of a chaotic FO-BLDC system. In this paper, the sliding surface is used to regulate the state of the BLDC system, which is known to exhibit chaotic behavior under certain conditions. By carefully designing the sliding surface, it is possible to control the system's dynamics and suppress chaotic behavior, leading to more predictable and stable operation. This is particularly important for practical applications of BLDC systems, where precise control over motor behavior is essential.

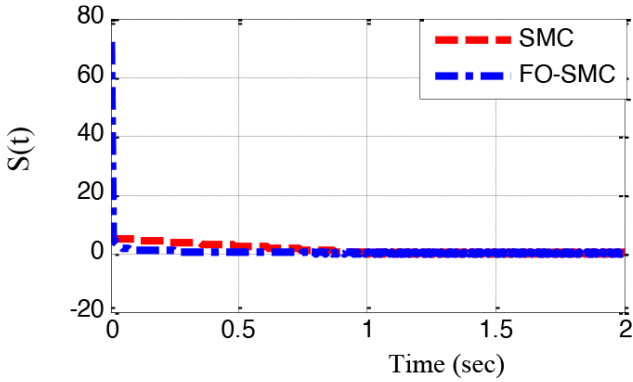


Figure 10. Sliding surface for state regulation of chaotic fractional-order BLDC system
Abbreviations: BLDC, Brushless direct control; FO-SMC, Fractional-order sliding mode controllers; SMC, Sliding mode controller

In Figure 11, which depicts the state rate trajectories of variable i_q , high-frequency oscillations can be observed in the rate of change of the second state variable when using the SMC method. However, this issue does not appear in the proposed method. The state rate trajectories of the variable i_q are important indicators of the behavior of the BLDC system, and the presence of high-frequency oscillations can negatively impact the system's performance and stability. The proposed method appears to provide a more effective means of regulating the state rates, resulting in smoother and more stable behavior of the BLDC system.

The analysis of Figures 10 and 11 demonstrates the effectiveness of the proposed FO-SMC in stabilizing the chaotic BLDC system while mitigating the adverse effects of external disturbances and parameter uncertainties. The sliding surface in Figure 10 ensures convergence of the state of the system by satisfying the Lyapunov stability criterion, thereby suppressing chaotic oscillations and enhancing the robustness. Compared to conventional SMC, the fractional-order approach significantly reduces high-frequency oscillations and chattering, leading to a smoother and more stable system response.

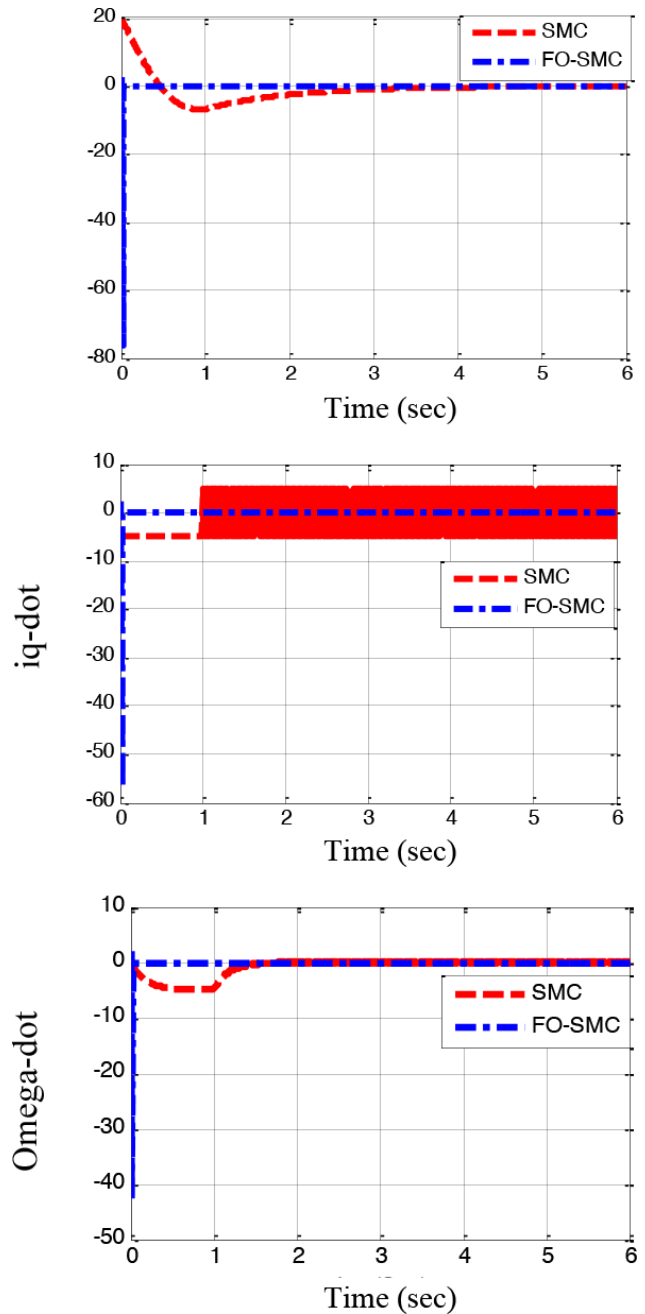


Figure 11. State rate trajectories regulation of variables i_d , i_q , and Ω in a fractional-order BLDC system using a fractional-order sliding mode control signal
Abbreviations: BLDC, brushless direct control; FO-SMC, fractional-order sliding mode controllers; SMC, Sliding mode controller

Additionally, Figure 8 highlights the improved regulation of state rate trajectories, showing that the FO-SMC strategy effectively minimizes fluctuations in i_d , i_q and Ω . This reduction in oscillations enhances the overall performance of the BLDC system by preventing excessive energy consumption and mechanical wear. Moreover, the method strongly resists uncertainties and external perturbations, ensuring reliable operation under practical conditions. These results confirm

that the proposed FO-SMC strategy outperforms conventional SMC, offering superior stability, robustness, and adaptability in controlling chaotic FO-BLDC systems.

To evaluate the performance of the controllers used in this paper, we use the following error metrics, which are the average sum of absolute errors:

$$\begin{cases} E_x = \frac{1}{T} \int_{T_0}^T (|e_{x_1}| + |e_{x_2}| + |e_{x_3}|) dt \\ E_{x-dot} = \frac{1}{T} \int_{T_0}^T (|e_{x_1-dot}| + |e_{x_2-dot}| + |e_{x_3-dot}|) dt \end{cases} \quad (35)$$

where $e_{x_1} = x_{1d} - x_1$, $e_{x_1-dot} = \dot{x}_{1d} - \dot{x}_1$, and $T = T_s.t_f$.

In Table 1, which presents the quantitative comparison of these two control methods, it can be observed that by calculating the average sum of absolute errors, the state regulation errors are somewhat close to each other, but there is a significant difference in the rate of change of state regulation errors, indicating the advantage and value of the proposed FO-SMC method.

4.2. Performance evaluation under parameter uncertainties and external disturbances

The FO-BLDC system with uncertainties and external disturbances is represented by Equation (36):

$$\begin{cases} {}_0D_t^{q_1} x_1 = -x_1 + x_2 x_3 \\ {}_0D_t^{q_2} x_2 = -x_2 - x_1 x_3 + \gamma x_3 + u(t) + \Delta g(x_1, x_2, x_3) + d(t) \\ {}_0D_t^{q_3} x_3 = -\sigma(x_3 - x_2) \end{cases} \quad (36)$$

where $\Delta g(x_1, x_2, x_3)$ refers to parameter uncertainties, and $d(t)$ refers to external disturbances. We aimed to observe the behavior and resistance of the system in response to these changes by applying them as inputs to the system. Moreover, these sentences are considered as the following equations:¹⁰

$$\begin{cases} \Delta g(x_1, x_2, x_3) = 10.75 \sin(10x_1(t)) \cos(3x_2(t)) \cos(\pi x_3(t)) \\ d(t) = 5.25 \cos(2x_2(t)) + 8.5 \sin(3t) \end{cases} \quad (37)$$

Now, similar to before, we consider the parameter vector as $(\mu, \gamma, \sigma) = (1, 20, 5.46)$, the homogeneous orders of the system as $q_1 = q_2 = q_3 = 0.995$, and $T_{sim} = 6$ sec. The time constant is $h = 0.005$, and the initial conditions as $(x_1(0), x_2(0), x_3(0)) = (5, 5, 5)$. A switching gain of $k = 5$ is used, and relation (32) is designed using the sign function based on the sliding mode control input. Its implementation in MATLAB software is used to plot the state paths, the state change rate, the control input, and the sliding

surface of the proposed method. A comparison is made with normal sliding mode control, which is naturally applied to the normal derivative system, to determine the advantages of the proposed method.

Observing Figure 12, it becomes apparent that the conventional sliding mode strategy results in a significant overshoot in the current i_d at the beginning of the period, which may cause the system to become saturated. Additionally, it can be observed that the current i_q in the conventional sliding mode strategy exhibits irregular, frequency-based oscillations over time, which reduces the system's overall performance quality. In contrast, the proposed method results in a completely smooth behavior. Therefore, the performance of the proposed method is more desirable. Furthermore, the Omega plot indicates that the superiority of the proposed method is evident, as it exhibits better convergence speed and fewer oscillations.

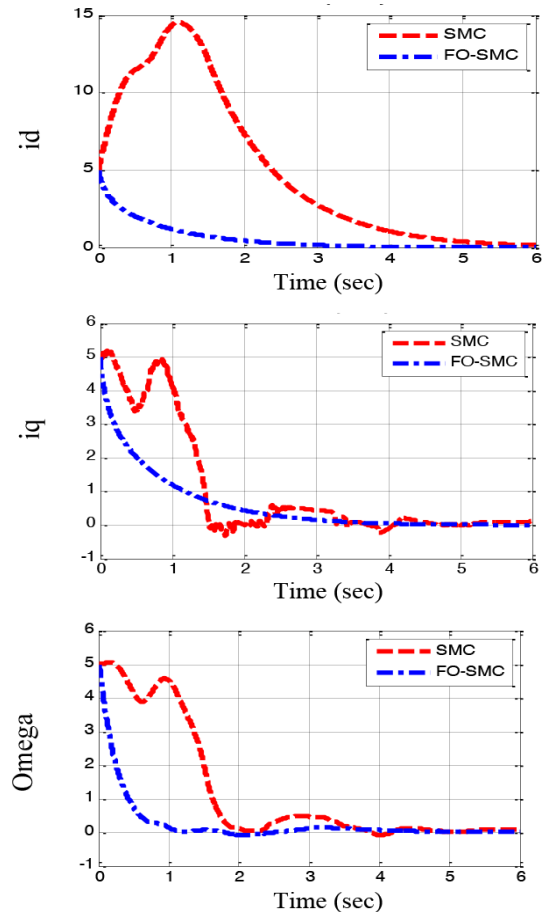


Figure 12. State trajectories regulation of i_d , i_q , and Omega variables in fractional-order BLDC system using FO-SMC signal in the presence of parameter uncertainties and external disturbances
Abbreviations: BLDC, brushless direct control; FO-SMC, fractional-order sliding mode controllers; SMC, sliding mode controller

Table 1. The average sum of absolute errors for state and rate of change of state regulation for fractional-order sliding mode control and conventional sliding mode control

The average sum of absolute errors.	State regulation error (E_x)	Rate of change of state regulation error (E_{x-dot})
SMC	7.2701	9.2106
FO-SMC	3.4487	0.1598

Abbreviations: FO-SMC, fractional-order sliding mode controllers; SMC, sliding mode controller.

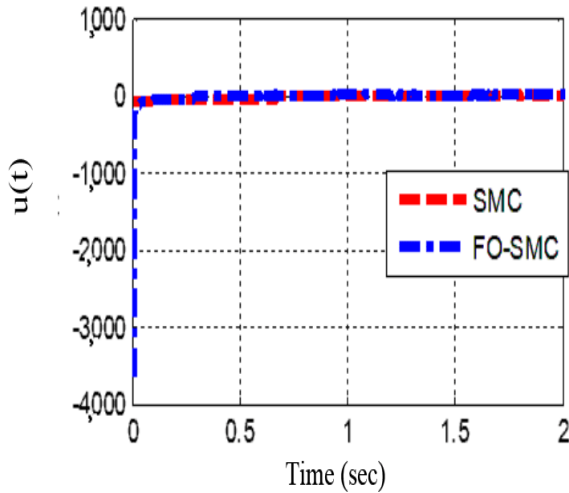


Figure 13. Effort for state regulation of fractional-order chaotic BLDC system in the presence of parameter uncertainties and external disturbances. Abbreviations: BLDC, brushless direct control; FO-SMC, fractional-order sliding mode controllers; SMC, sliding mode controller

According to Figure 13, it is clear that the proposed FO-SMC method for the FO-BLDC system requires higher initial energy for control, which, of course, imposes limitations on this method. However, if necessary, this limitation can be constrained by using a limiter on the energy.

Figure 14 illustrates the behavior of the sliding surface in the presence of parametric uncertainties and external disturbances, emphasizing the robustness of the proposed FO-SMC. The sliding surface is a crucial element in control theory, playing a key role in stabilizing the chaotic FO-BLDC system under uncertain conditions. Unlike conventional SMC, which suffers from significant fluctuations and delayed convergence in the presence of uncertainties, the fractional-order sliding surface effectively reduces oscillations and accelerates state stabilization. This enhanced performance is due to the memory effect of fractional calculus, which improves system adaptability and ensures smoother control actions. By mitigating instability and enhancing robustness, the FO-SMC approach provides a more stable and

efficient control strategy, making it highly suitable for real-world applications where uncertainties and disturbances are inevitable.

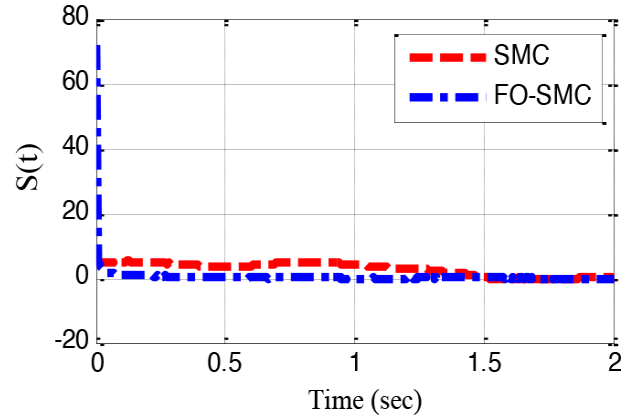


Figure 14. Sliding surface for state regulation of a fractional-order chaotic BLDC system in the presence of parameter uncertainties and external disturbances. Abbreviations: BLDC, brushless direct control; FO-SMC, fractional-order sliding mode controllers; SMC, sliding mode controller

As seen in Figure 15, the proposed method achieves negligible convergence time and convergence error, unlike the conventional SMC method, in which the convergence of the sliding surface is undesirable. This highlights the superiority of the proposed method in providing more stable and predictable control of the BLDC system, even in the presence of parameter uncertainties and external disturbances. This figure illustrates the state rate trajectories of a BLDC system under the sliding mode control method and the proposed method. In the sliding mode control method, significant oscillations are observed in the rate of change of the first state variable ($i_d - dot$), which can negatively affect the current regulation of the system. However, this issue is not present in the proposed method. In addition, as shown in this figure, high-frequency oscillations and significant changes in the amplitude of the rate of change of the second state variable ($i_q - dot$) occur generated under the SMC method, which can be destructive for the current regulation of the system. However, these issues are not present in the proposed method. Furthermore, it is observed that relatively high-amplitude

oscillations with significant changes in the rate of change of the third state variable ($\Omega - \dot{\text{dot}}$) over time occur under the sliding mode control method, which can be destructive for the frequency regulation of the system. However, these issues are not present in the proposed method. These observations highlight the superiority of the proposed method in regulating the state rates of the BLDC system with smoother and more stable behavior compared to the sliding mode control method.

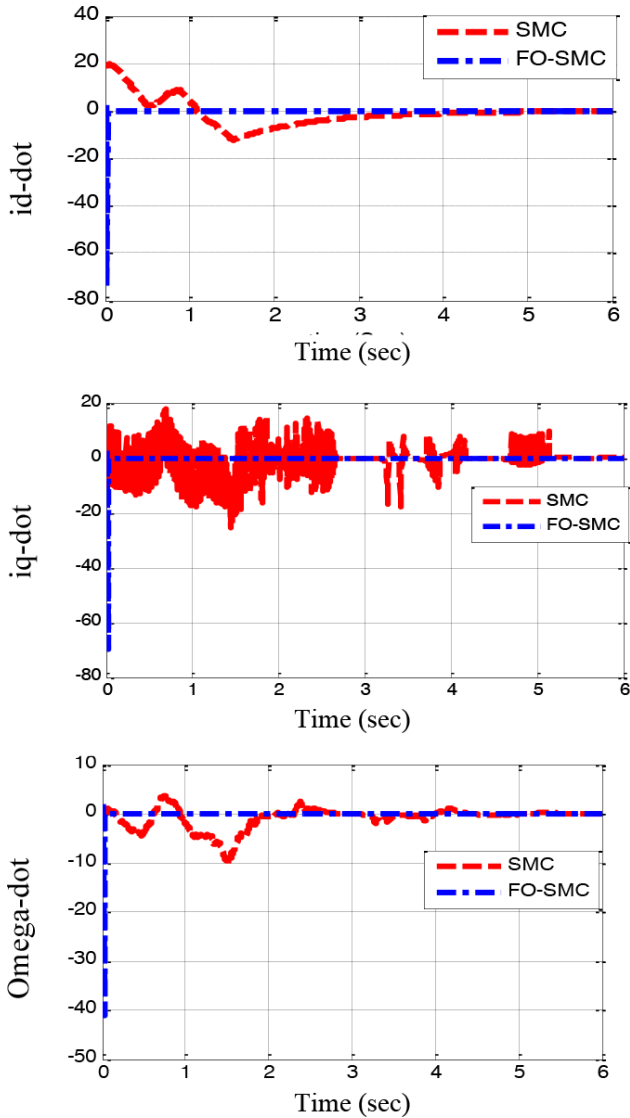


Figure 15. State rate trajectory regulation of variables i_d , i_q , and Ω in the FO-BLDC system using the FO-SMC signal in the presence of parameter uncertainties and external disturbances. Abbreviations: BLDC, brushless direct control; FO-SMC, fractional-order sliding mode controllers; SMC, Sliding mode controller

In Table 2, which presents the quantitative comparison of these two control methods in the presence of parameter uncertainties and external disturbances, it is observed that the average sum

of absolute error values indicates a significant increase in the state regulation error in the conventional SMC method compared to Table 1, while this increase is only 0.05 in the proposed method. In the section on the rate of change in the state regulation error, the state regulation error value in the conventional SMC method has increased by one unit compared to Table 1, while this increase is only 0.007 in the proposed method. This demonstrates the significant advantage and resistance of the proposed FO-SMC method compared to the already robust conventional sliding mode method, which is itself preferable to, for example, the PID method.

In general, the superiority of SMC over PID and FO-SMC over FOPID in controlling chaotic BLDC motor systems can be justified based on several critical performance factors. SMC provides robust control under parameter uncertainties and external disturbances, ensuring stable operation where PID controllers require continuous tuning and struggle with nonlinearities inherent in BLDC motors. Additionally, SMC guarantees finite-time convergence, whereas PID controllers only achieve asymptotic stability, often resulting in longer settling times and susceptibility to steady-state errors.

On the other hand, FO-SMC further improves upon SMC by reducing the chattering effect, which is a major issue in conventional sliding mode controllers. The fractional-order nature of FO-SMC introduces memory effects, offering greater flexibility in parameter tuning and enhanced adaptability to system variations. This results in a smoother control action and improved dynamic response compared to FOPID, which, despite its fractional-order terms, still relies on PID-based tuning strategies that can be computationally expensive and sensitive to high-frequency oscillations.

The comparative analysis confirms that FO-SMC is the most effective approach for chaotic BLDC motor control, as it provides higher stability, faster response times, and greater resilience to uncertainties compared to the other methods. These advantages make FO-SMC a superior choice for real-world BLDC applications requiring precise control, reduced energy consumption, and improved system reliability.

The simulation results presented in Figures 12 and 13 demonstrate the superiority of FO-SMC over conventional SMC in handling uncertainties. The conventional SMC exhibits significant overshoot and irregular oscillations in the controlled variables i_d , i_q , and Ω , which

Table 2. The average sum of absolute errors for state and rate of change of state regulation for fractional-order sliding mode control and conventional sliding mode control in the presence of parameter uncertainties and external disturbances

The average sum of absolute errors.	State regulation error (E_x)	Rate of change of state regulation error (E_{x-dot})
SMC	7.2701	9.2106
FO-SMC	3.4487	0.1598

Abbreviations: FO-SMC, fractional-order sliding mode controllers; SMC, sliding mode controller.

may lead to performance degradation and excessive energy consumption. Conversely, FO-SMC achieves a more stable state trajectory, effectively suppressing oscillations and ensuring faster convergence to the desired operating point. This is attributed to the fractional-order terms, which introduce an additional degree of freedom, enabling the controller to adapt dynamically to variations in system parameters.

Additionally, Figures 14 and 15 further validate the enhanced stability and robustness of FO-SMC in regulating the sliding surface and state rate trajectories under uncertain conditions. The sliding surface in FO-SMC converges significantly faster than conventional SMC, ensuring improved tracking accuracy and predictable system behavior. Moreover, Table 2 quantitatively confirms the advantage of FO-SMC, with a notable reduction in the state regulation error (from 7.2701 in SMC to 3.4487 in FO-SMC) and a drastic decrease in the rate of change of state regulation error (from 9.2106 in SMC to 0.1598 in FO-SMC). These results highlight the robustness of the FO-SMC, proving that it reduces steady-state error, and ensure smoother transient response and lower energy consumption in the presence of disturbances.

5. Conclusion

One of the key challenges in nonlinear control systems, particularly in BLDC motors, is their susceptibility to parameter uncertainties and external disturbances. Traditional SMC techniques, while offering strong robustness, tend to suffer from high-frequency oscillations (chattering) and degraded performance when exposed to uncertainties. In contrast, FO-SMC leverages the memory effect of fractional calculus to provide a smoother control response while maintaining strong disturbance rejection capabilities. In this study, a FO-SMC was designed to regulate the chaotic behavior of a FO-BLDC system. The system was effectively driven toward its equilibrium point by carefully selecting an appropriate sliding surface and a suitable control input, mitigating chaotic oscillations.

Sliding mode control is widely recognized for its robustness against uncertainties and external disturbances, making it a preferred choice for nonlinear systems. However, a major drawback of conventional SMC is the chattering phenomenon, particularly in high-speed dynamic systems. Our analysis revealed that while SMC successfully stabilized the system in finite time, it also introduced significant fluctuations in x_1 and x_1 -dot states. To address this limitation, FO-SMC was implemented, leading to a smoother system response and reduced state oscillations. Additionally, FO-SMC improved system adaptability and enhanced resistance to uncertainties and disturbances.

The superiority of FO-SMC over conventional SMC was demonstrated through both qualitative (graphical) and quantitative (Tables 1 and 2) comparisons. The key advantages of the proposed approach are summarized as follows:

- Fractional-order integration enhances stability: Transforming the system into a fractional-order framework inherently introduces a fractional-order integration operation, which helps reduce system errors and improves stability.
- Innovative hybrid control strategy: Unlike conventional methods, the proposed FO-SMC approach integrates a linear continuous term alongside relay control (as described in Equation (32)), resulting in smoother control behavior and significantly reducing chattering effects.
- Improved adaptability and robustness: Leveraging fractional-order dynamics in the controller significantly enhances the system's adaptability while increasing its resilience to parameter uncertainties and external disturbances.

These findings highlight the effectiveness of fractional-order control methodologies in suppressing chaotic behaviors, ensuring smooth operation, and enhancing the robustness of nonlinear systems. The proposed FO-SMC framework

presents a viable solution for improving stability, efficiency, and control precision in practical BLDC motor applications.

Acknowledgments

None.

Funding

None.

Conflict of interest

The authors declare they have no competing interests.

Author contributions

Conceptualization: Amin Kaveh, Mohammad Vahedi

Formal analysis: Mohammad Vahedi, Majid Gandomkar

Investigation: Amin Kaveh

Methodology: Mohammad Vahedi

Writing – original draft: Amin Kaveh




Writing – review & editing: Mohammad Vahedi, Majid Gandomkar

Availability of data

All data is presented in this paper.

References

- Xia C. *Permanent Magnet Brushless DC Motor Drives and Controls*. John Wiley & Sons; 2012.
- Jabbar MA, Phyu HN, Liu Z, Bi C. Modeling and numerical simulation of a brushless permanent-magnet DC motor in dynamic conditions by time-stepping technique. *IEEE Trans Ind Appl*. 2004;40(3):763-770. <https://doi.org/10.1109/TIA.2004.826330>.
- Qi G. Energy cycle of brushless DC motor chaotic system. *Appl Math Model*. 2017;51:686-697. <https://doi.org/10.1016/j.apm.2017.06.001>.
- Utkin VI. *Sliding Modes in Control and Optimization*. Springer; 1992.
- DeCarlo RA, Zak SH, Matthews GP. Variable structure control of nonlinear multivariable systems: a tutorial. *Proc IEEE*. 1998;76(3):212-232. <https://doi.org/10.1109/5.2070>.
- Zhou P, Bai R, Zheng JM. Stabilization of a fractional-order Chaotic brushless DC Motor via a Single Input. *Nonlinear Dyn*. 2015;(82):519-525. <https://doi.org/10.1007/s11071-015-2452-2>.
- Li S, Li P, Zheng Z, Huang T. Fractional order sliding mode control for circulating current suppressing of MMC. *Electr Eng*. 2023;105(6):3791-3800. <https://doi.org/10.1007/s00202-023-01902-7>.
- Petras I. *Fractional-Order Nonlinear Systems: Modeling, Analysis, and Simulation*. Springer; 2011.
- Hilfer R. *Applications of Fractional Calculus in Physics*. World Scientific Pub. Co.; 2000.
- Shahzad M. Chaos control in three dimensional cancer model by state space exact linearization based on Lie Algebra. *Int J Eng Technol*. 2016;4(33):1-11. <https://doi.org/10.14419/ijet.v4i3.6129>.
- Xue G, Lin F, Qin B. Adaptive neural network control of chaotic fractional order permanent magnet synchronous motors using backstepping technique. *Front Phys*. 2020;8:12. <https://doi.org/10.3389/fphy.2020>.
- Ge Z, Lin G. The complete, lag and anticipated synchronization of a BLDCM chaotic system. *Chaos, Solitons & Fractals*. 2007;34:740-764. <https://doi.org/10.1016/j.chaos.2006.05.057>.
- Hemati N. Strange attractors in brushless DC motors. *IEEE Trans Circuits Syst I Fundam Theory Appl*. 1994;41(1):40-45. <https://doi.org/10.1109/81.265867>.
- Ye S, Chau KT. Chaotization of DC motors for industrial mixing. *IEEE Trans Ind Electron*. 2007;54:2024-2032. <https://doi.org/10.1109/TIE.2007.903252>.
- Reyes R, Cruz C, Nakano-Miyatake M, Perez-Meana H. Digital video watermarking in DWT domain using chaotic mixtures. *IEEE Lat Am Trans*. 2010;8:304-310. <https://doi.org/10.1109/TLA.2010.5438444>.
- Rajagopal K, Vaidyanathan S, Karthikeyan A, Duraisamy P. Dynamic analysis and chaos suppression in a fractional order brushless DC motor. *Electr Eng*. 2016;99:721-733. https://doi.org/10.1007/978-3-319-32273-5_2.
- Sun LX, Lu S, Wen ZG, Li YF. Analysis of chaotic motion mechanism of permanent magnet synchronous motors. *Electr Mach Control*. 2019;23(3):97-104. <https://doi.org/10.16383/j.aemc.2019.3.001>.
- Wu S, Zhang JA. Terminal sliding mode observer based robust backstepping sensorless speed control for interior permanent magnet synchronous motor. *Int J Control Autom Syst*. 2018;16(6):2743-2753. <https://doi.org/10.1007/s12555-016-0782-x>.
- Tang C, Bai L, Zhang G, Yang J, Li T. Robust guaranteed cost control of PMSM chaotic system with uncertain parameters. *J Eng Sci Technol Rev*. 2020;13(3):181-190. <https://doi.org/10.25103/jestr.133.01>.
- Yu X, Zhang C. Robust fractional-order PID control for chaotic systems. *Nonlinear Dyn*. 2021;103(2):1123-1140. <http://dx.doi.org/10.2139/ssrn.5162779>.
- Kumar R, Singh M. Comparative study of PID, FOPID, and sliding mode control for uncertain systems. *IEEE Access*. 2020;8: 76523-76535. <https://doi.org/10.31763/ijrcs.v5i1.1764>.

22. Mendel JM. *Uncertain Rule-Based Fuzzy Logic Systems: Introduction and New Directions*. Springer; 2017. <https://doi.org/10.1109/MCI.2007.357196>.
 23. El-Bardini M, El-Nagar AM. Interval Type-2 Fuzzy Control Design for Uncertain Nonlinear Systems. *ISA Trans.* 2014; 53(3):732-743. <https://doi.org/10.1016/j.isatra.2014.02.007>.
 24. Huerta-Moro S, Tavizón-Aldama JD, Tlelo-Cuautle E. FPGA implementation of sliding mode control and proportional-integral-derivative controllers for a DC–DC buck converter. *Technologies.* 2024;12(10):184. <https://doi.org/10.3390/technologies12100184>.
 25. Roy P, Ray S, Bhattacharya S. Control of chaos in brushless DC motor design of adaptive controller following back-stepping method. In: *International Conference on Control, Instrumentation, Energy & Communication (CIEC)* ; 2014. <https://doi.org/10.1109/CIEC.2014.107>.
 26. Patra A, Chakrabarty K, Nag T. Control of Chaos in BLDC Motor Drive. In: *Proceedings of IEEE, Applied Signal Processing Conference (ASPCON)*; 2018. <https://doi.org/10.1109/ASPCON.2018.8605733>.
 27. Yaz M, Cetin E. Brushless Direct Current Motor Design and Analysis. *COJ Electronics & Communications*; 2021. <https://doi.org/10.31031/COJEC.2021.05.000602>.
 28. Hung JY, Gao W, Hung JC. Variable structure control: a survey. *Procs of the IEEE.* 1993;40(1):2-20. <https://doi.org/10.1109/5.210201>.
 29. Xue G, Lin F, Qin B. Adaptive neural network control of chaotic fractional order permanent magnet synchronous motors using backstepping technique. *Front Phys.* 2020;8. <https://doi.org/10.3389/fphy.2020.00062>.
- Amin Kaveh** received his Bachelor's degree in Electrical Engineering and Telecommunications from the Islamic Azad University, Najaf Abad Branch in Iran, in 2006 and his Master's degree from Khomeini Shahr University in Iran in 2012. He has been a Ph.D. candidate in Electrical Engineering and Control at the Islamic Azad University, Saveh Branch in Iran, since 2015. Currently, he is working as a researcher in the field of control engineering, focusing on nonlinear system control.
 <http://orcid.org/0009-0000-6720-2510>
- Mohammad Vahedi** received his Bachelor's degree from Amirkabir University of Technology in Iran in 2004 and his Master's degree from Shiraz University in Iran in 2007. He then obtained his Ph.D. in Mechanical Engineering from Iran University of Science and Technology in 2014. He is currently an assistant professor and faculty member at the Islamic Azad University in Iran. His research interests include control of nonlinear systems, robotics, and intelligent control.
 <http://orcid.org/0000-0003-1834-8577>
- Majid Gandomkar** is an Associated Professor in the University of Islamic Azad University, Saveh, Iran.
 <https://orcid.org/0000-0001-6199-1483>

An International Journal of Optimization and Control: Theories & Applications
(<https://accscience.com/journal/ijocta>)



This work is licensed under a Creative Commons Attribution 4.0 International License. The authors retain ownership of the copyright for their article, but they allow anyone to download, reuse, reprint, modify, distribute, and/or copy articles in IJOCTA, so long as the original authors and source are credited. To see the complete license contents, please visit <http://creativecommons.org/licenses/by/4.0/>.